
Spherical wave AVO-modelling in elastic isotropic media

Arnim B. Haase and Charles P. Ursenbach

ABSTRACT

The AVO-response of two-layer isotropic models for AVO-Classes 1, 2, 3 and 4 is investigated for converted waves. Zoeppritz's reflection coefficients and the Weyl/Sommerfeld-integral are utilized for the computations. Spherical wave results for R_{ps} and R_{pp} are compared with plane wave reflectivity. Depth dependence of spherical wave AVO is found to be strongest near critical angles of Classes 1 and 2. There is some similarity between R_{ps} and R_{pp} for Classes 1 and 2. Normalized Class 3 and 4 responses show no depth dependence. There is no similarity between Class 3 R_{ps} and R_{pp} .

INTRODUCTION

AVO-analysis and AVO-inversion are widely accepted tools in seismic exploration. The common approach is plane-wave analysis, and linear approximations of the Zoeppritz equations are utilized to this end. For these approximations small incidence angles and small parameter changes are assumed. In recent years, three-parameter AVO-inversion has been investigated for the extraction of density information (e.g. Downton and Lines, 2001). It was observed that, for reasonably accurate density estimates, larger offsets/angles are required than normally used for two parameter inversion, preferably even postcritical events if present. Linearized approximations begin to break down at larger angles and are not applicable near critical points. Even "exact Zoeppritz" is a plane wave approximation to the real world. Winterstein and Hanten (1985) show that cylindrical wave modeling results in a much better fit of seismic data than does plane wave modeling near critical angles. Instead of the amplitude jump at the critical angle predicted by plane-wave theory, they find a more gradual amplitude transition for cylindrical wave models and actual data. In order to increase the accuracy of AVO-inversion, joint PP-PSv inversion has been suggested and investigated (see for example Margrave et al., 2001). The question arises as to what the spherical wave AVO-response of converted waves might be. This modeling study attempts to provide some answers to this question and investigates the spherical wave AVO-response of converted waves for AVO-Classes 1, 2, 3 and 4.

THEORY

Plane-wave particle motion reflection and transmission coefficients for elastic isotropic media in welded contact are given by Zoeppritz's equations. The formalism for expressing spherical wave fronts as contour integrals over plane waves goes back to Weyl (1919). Aki and Richards (1980, p217) derive equations for generalized PP-reflections and generalized PSv-reflections in terms of potentials Φ (Equation 1) and Ψ (Equation 2):

$$\Phi = Ai \omega e^{-i\omega t} \int_0^{\infty} R_{pp} \frac{p}{\xi} J_0(\omega pr) e^{i\omega \xi (z+h)} dp \quad (1)$$

$$\Psi = Ai \omega e^{-i\omega t} \int_0^{\infty} \left(\frac{1}{i\omega p} \frac{\beta}{\alpha} R_{ps} \right) \frac{p}{\xi} J_0(\omega pr) e^{i\omega(\xi h + \eta z)} dp \quad (2)$$

Reflections from an elastic interface are computed firstly by introducing particle motion reflection coefficients given by Zoeppritz's equations. Secondly, particle motion \mathbf{u} is computed from

$$u = \nabla \Phi + \nabla \times \nabla \times (0, 0, \Psi) \quad (3)$$

and from the potentials given by Equations (1) and (2). Thirdly, normalization by the maximum particle motion magnitude for unit reflectivity leads to the spherical wave PP and PSv reflection coefficients. The integrations shown in Equations (1) and (2) proceed one frequency point at a time. When all frequency points are computed for the desired output bandwidth, the time domain response is found by inverse Fourier transform. Quadrature traces are determined by Hilbert transform. From these two trace types amplitude and phase of reflected spherical waves can be calculated

MODELLING

An actual gas-sand reservoir from the prairies is utilized to derive two layer models for this study. Density ρ_1 is 2400 kg/m^3 for the layer just above the reservoir. P-wave velocity $\alpha_1 = 2000 \text{ m/s}$ is dictated by a reservoir depth of 500m and a corresponding two-way travel-time of approximately 500ms. The layer parameters for AVO-Classes 1, 2 and 3 shown in Table 1 are adapted from Rutherford and Williams (1989). Class 4 parameters are adapted from Castagna et al. (1998). Output signal bandwidth and linear edge tapers are determined by choosing a 5/15-80/100 Hz Ormsby wavelet as the source signature. Free surface effects are not considered in this study. A P-wave point source and spherical wave fronts are assumed for the computations.

Table 1. Layer Parameters.

Class	α_1 /[m/s]	β_1 /[m/s]	ρ_1 /[kg/m ³]	α_2 /[m/s]	β_2 /[m/s]	ρ_2 /[kg/m ³]
1	2000	879.88	2400	2933.33	1882.29	2000
2	2000	879.88	2400	2400	1540.05	2000
3	2000	879.88	2400	1963.64	1260.04	2000
4	2000	1000	2400	1598.77	654.32	2456.43

Figures 1 through 4 show AVO-response magnitudes computed from trace envelopes. AVO-Class 1 comparisons are given in Figure 1a (for converted waves) and Figure 1b (for PP-waves). Similarly, AVO-Class 2 through 4 results are shown in Figures 2 through 4. Plane wave comparisons are added to all AVO magnitude responses in order to highlight the impact of spherical wave fronts. Figures 5 through 8 display spherical wave PS and PP-reflection traces for AVO Classes 1 through 4. These trace displays are scaled

individually in order to accommodate maximum amplitudes. Clipping of maximum trace amplitudes is indicated by colour changes.

DISCUSSION AND CONCLUSIONS

Figure 9 shows scaling comparisons for Class 1 PP-AVO. The layer parameters for Class 1 AVO in Table 1 give a plane wave zero offset reflection coefficient of 0.1. Normalizing the zero offset spherical wave response to 0.1 gives good agreement with the plane wave response up to about 30 degrees incidence angle. Spherical spreading can be compensated for by $1/\cos$ -scaling. Applying $1/\cos$ -scaling to the spherical wave response brings it much closer to a plane wave comparison at angles well beyond critical. All normalization factors used to compute Figures 1 through 4 are derived by setting reflection coefficients R in Equations 1 and 2 to unity. Inspection of Figures 1b and 9, shows that unity- R scaling provides the highest level of agreement between spherical wave responses and plane wave responses.

For Class 1 AVO-models, P-wave and S-wave velocities are increasing across the interface as can be seen in Table 1. Because of this velocity increase critical angles exist and head waves are generated in Class 1 models. A head wave can be seen separating from reflected waves at the highest angles in Figure 5a. It also exists in Figure 5b, but is not as evident for the angles shown. The PSv-reflection traces in Figure 5a start with zero amplitude at zero angle. Then a negative reflection (-180 degrees of angle) grows stronger towards a magnitude maximum just below 30 degrees. Beyond 30 degrees the PSv-reflection strength diminishes first and then goes through a 90 degree phase rotation and increasing strength near the critical angle just beyond 40 degrees. With angles increasing beyond that, amplitudes diminish towards zero at 90 degrees and the phase angle returns to -180 degrees. Figure 1a shows the magnitude of R_{ps} for Class 1. The greatest departure from a plane wave comparison is observed in the vicinity of the critical angle. The larger the reflector depth, the closer the spherical response to the plane wave comparison; however, even at 2000m depth, there are significant differences. The Class 1 PP-reflection comparison in Figure 1b bears striking similarities to its PSv counterpart in the way it differs from plane wave behavior near the critical angle. The depth dependence of spherical wave Class 1 AVO-responses of R_{ps} and R_{pp} is quite similar (including a phase rotation near the critical angle). The Class 2 comparison in Figures 2a and 2b shows the same plane wave departure near the critical angle as does Class 1.

Figure 10 displays the frequency dependence of AVO-Class 1 spherical wave PP reflection coefficients. Integration over frequency as part of the inverse Fourier transform appears to greatly reduce the high angle ripple well beyond the critical angle. Similar undulations changing with frequency can be seen in numerical examples for spherical waves given by Macdonald et al. (1987). An increasing departure from the high frequency behaviour can also be observed around the critical angle toward lower frequencies. This departure is thought to be caused by the near field term, which increases in importance with increasing wavelength-to-depth ratio.

Results of AVO-Class 3 modeling are very different when compared to Class 1. Table 1 shows a P-wave velocity inversion, only S-wave velocities increase across the interface. There is no head wave (and no phase rotation) because there is no critical angle for

incident P-waves. Another interesting observation is the apparent lack of depth dependence. The reasons for this apparent depth independence of Class 3 spherical wave AVO-responses are firstly the normalization and secondly the equal angle displays. Away from the critical angle the Class 1 response is also increasingly independent of depth. Class 3 R_{ps} in Figure 3a starts off from zero and turns negative first, as before in Figure 1a (see also Figure 5a). By contrast to Class 1, it goes through zero at about 60 degrees of angle and turns positive. Similar to Class 1 R_{ps} , reflection strength returns to zero when approaching 90 degrees. There is no departure from a plane wave comparison. Class 3 R_{pp} (Figure 3b) is always negative and nonzero for any angle. There is no apparent similarity between Class 3 R_{ps} and R_{pp} .

Results of AVO-Class 4 modeling are similar to Class 3. Inspection of Table 1 shows that both, P-wave velocities and S-wave velocities decrease across the interface. There are no critical angles. As is the case for Class 3 results, there is no departure from plane wave comparisons for Class 4 either. Class 4 R_{ps} is stronger than Class 3 R_{ps} but has no zero crossing.

REFERENCES

- Aki, K.T., and Richards, P.G., 1980, Quantitative Seismology: Theory and Methods: Vol. 1, W.H. Freeman and Co.
- Castagna, J.P., Swan, H.W., and Foster, D.J., 1998, Framework for AVO gradient and intercept interpretation: *Geophysics*, **63**, 948-956.
- Downton, J.E., and Lines, L.R., 2001, Constrained three parameter AVO inversion and uncertainty analysis: 71st Ann. SEG Mtg., Expanded Abstracts, 251-254.
- Macdonald, C., Davis, P.M., and Jackson, D.D., 1987, Inversion of reflection travel times and amplitudes: *Geophysics*, **52**, 606-617.
- Margrave, G.F., Stewart, R.R., and Larsen, J.A., 2001, Joint PP and PS seismic inversion: The Leading Edge, **20**, No. 9, 1048-1052.
- Rutherford, S.R., and Williams, R.H., 1989, Amplitude-versus-offset variations in gas sands: *Geophysics*, **54**, 680-688.
- Weyl, H., 1919, Ausbreitung elektromagnetischer Wellen ueber einem ebenen Leiter: *Ann. Physik*, **60**, 481-500.
- Winterstein, D.F., and Hanten, J.B., 1985, Supercritical reflections observed in P- and S-wave data: *Geophysics*, **50**, 185-195.

ACKNOWLEDGEMENTS

Thank you to Professor E. Krebes for his help with the theory. Support by the CREWES team and its industrial sponsorship is gratefully acknowledged.

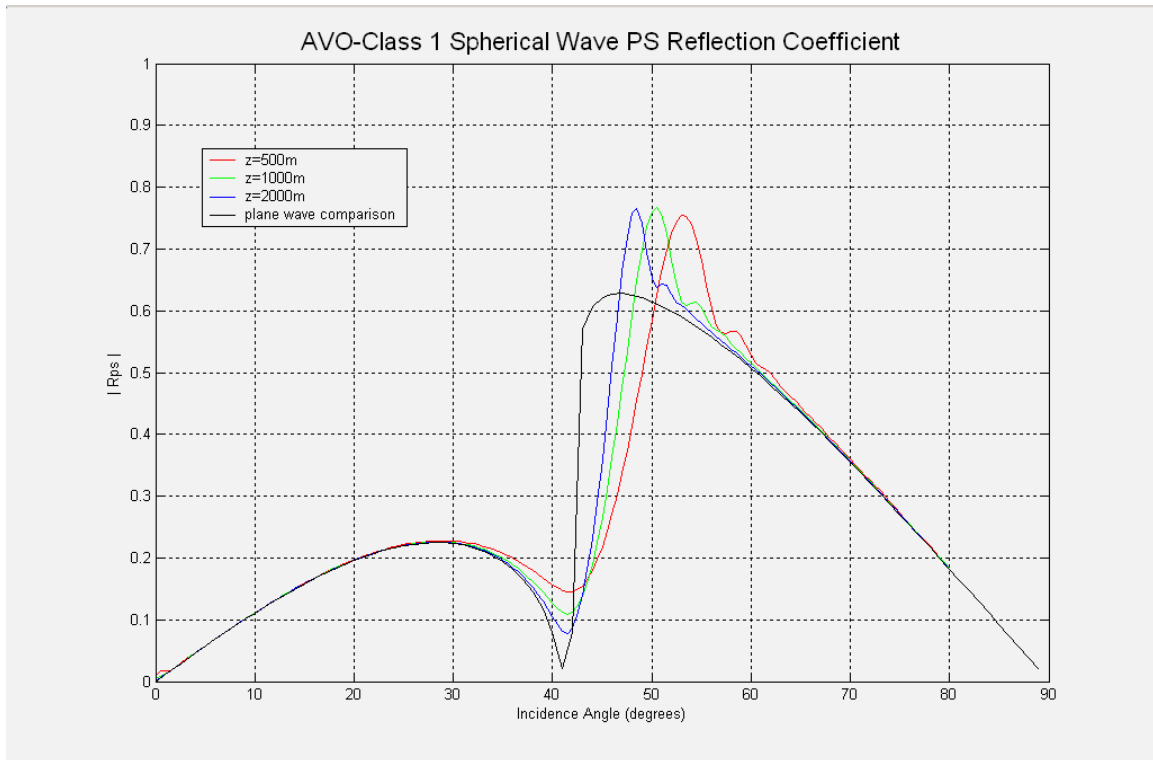


FIG. 1a. PS reflection coefficient curves for Class 1 AVO.

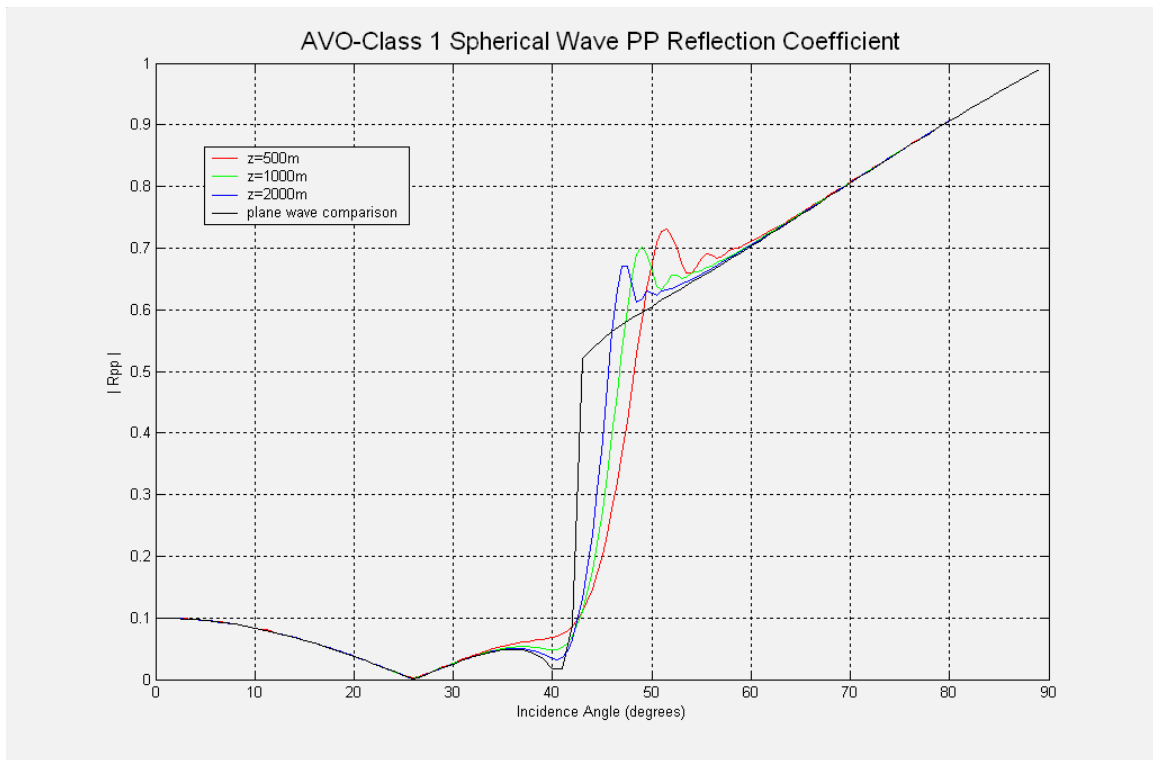


FIG. 1b. PP reflection coefficient curves for Class 1 AVO.

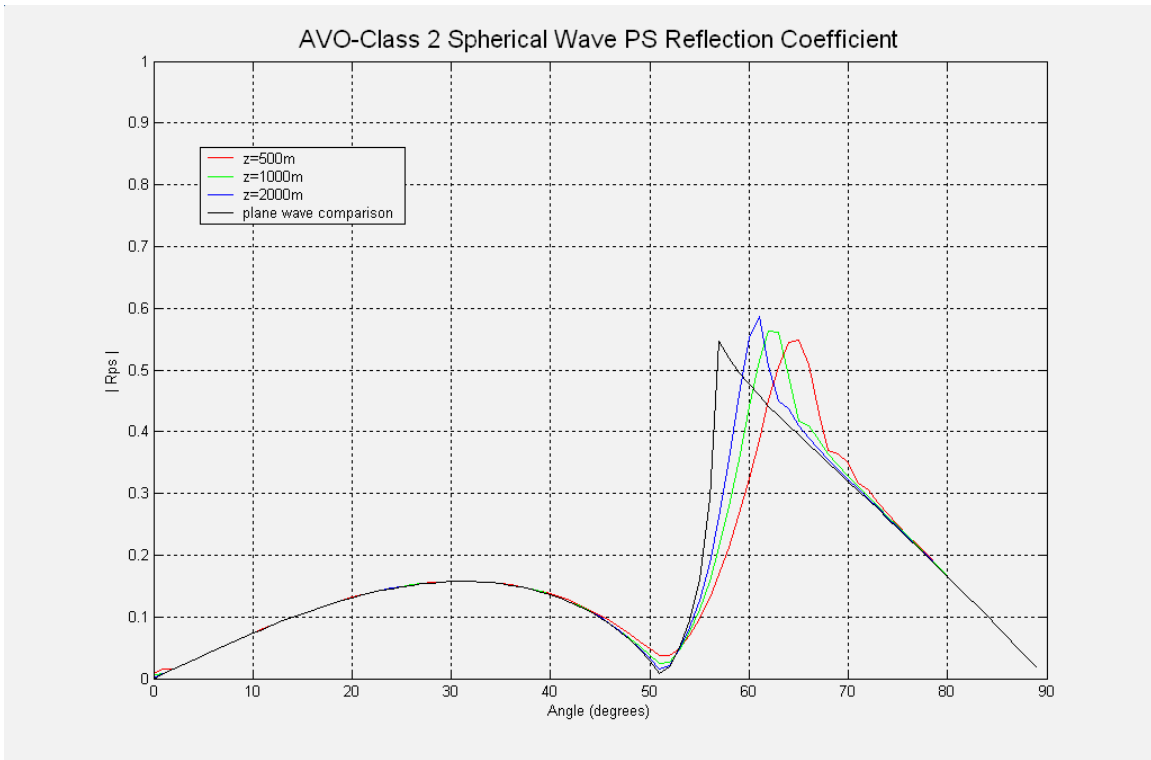


FIG. 2a. PS reflection coefficient curves for Class 2 AVO.

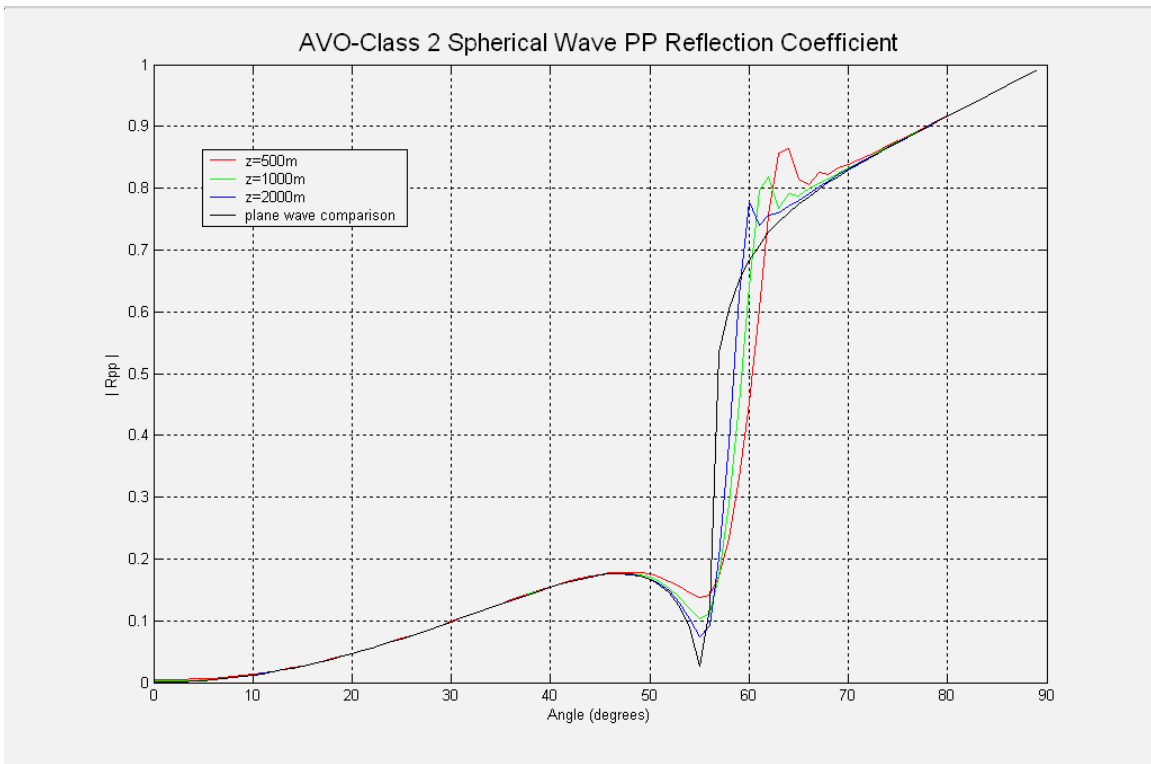


FIG. 2b. PP reflection coefficient curves for Class 2 AVO.

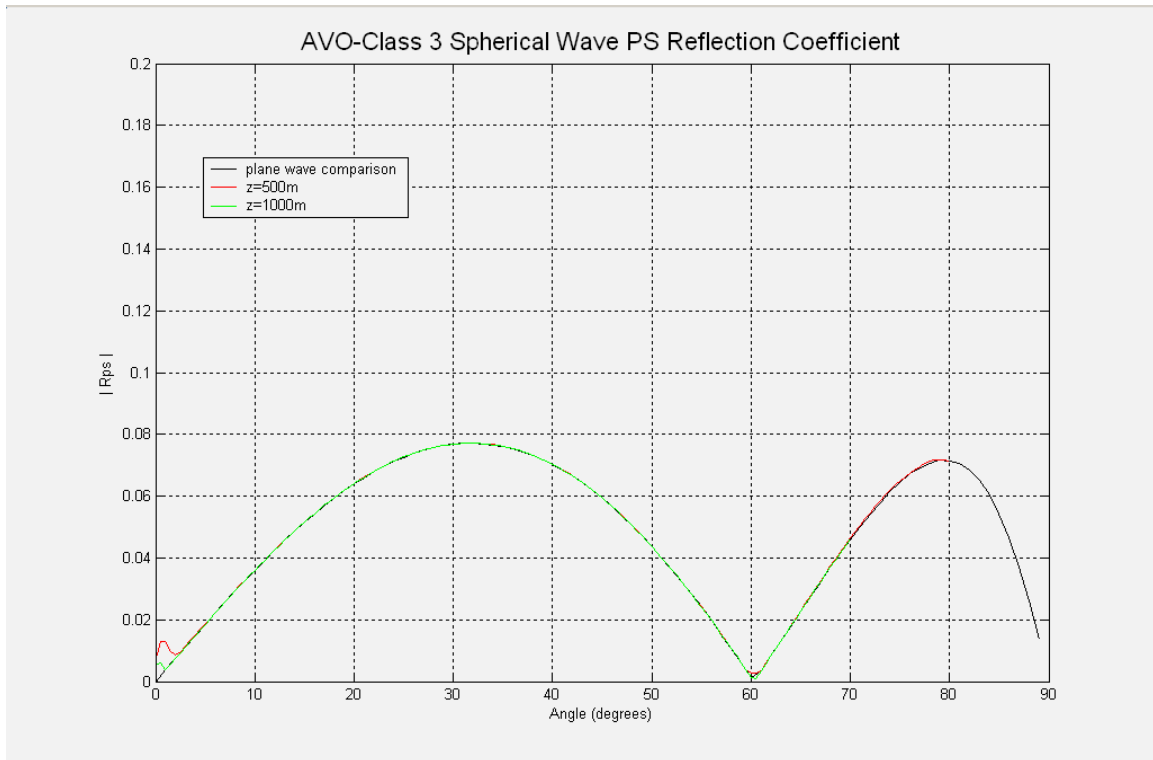


FIG. 3a. PS reflection coefficient curves for Class 3 AVO

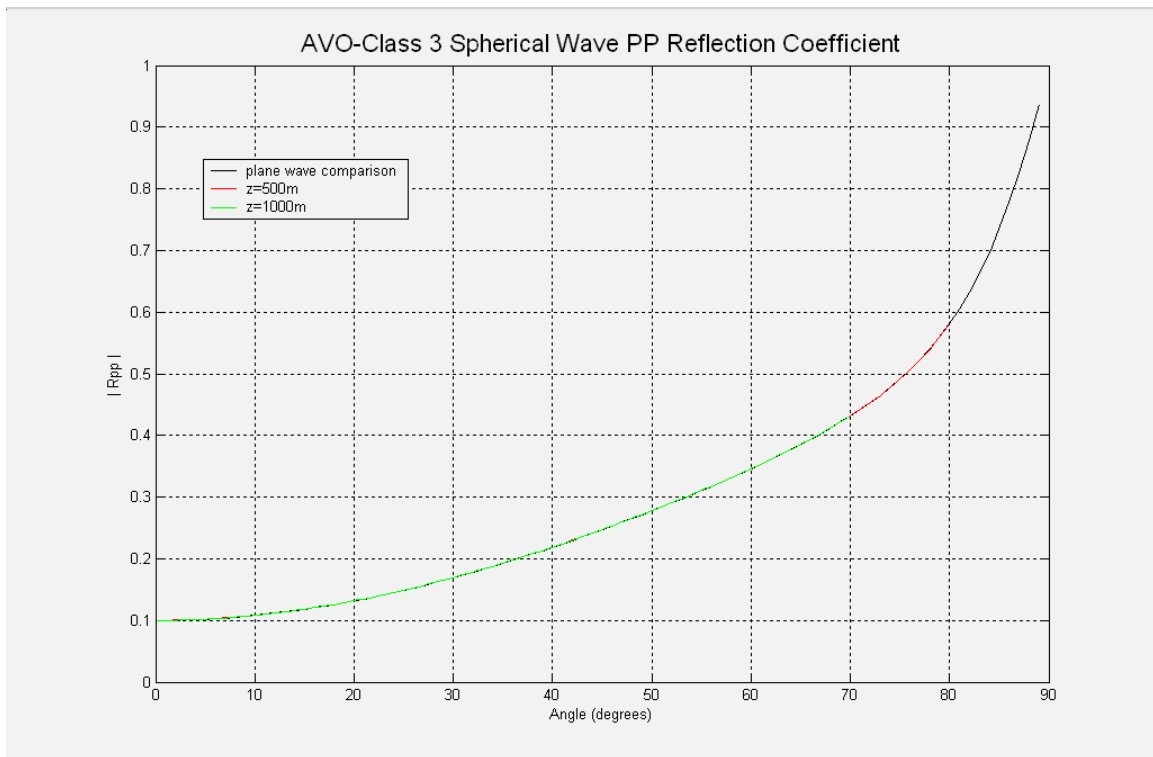


FIG. 3b. PP reflection coefficient curves for Class 3 AVO.

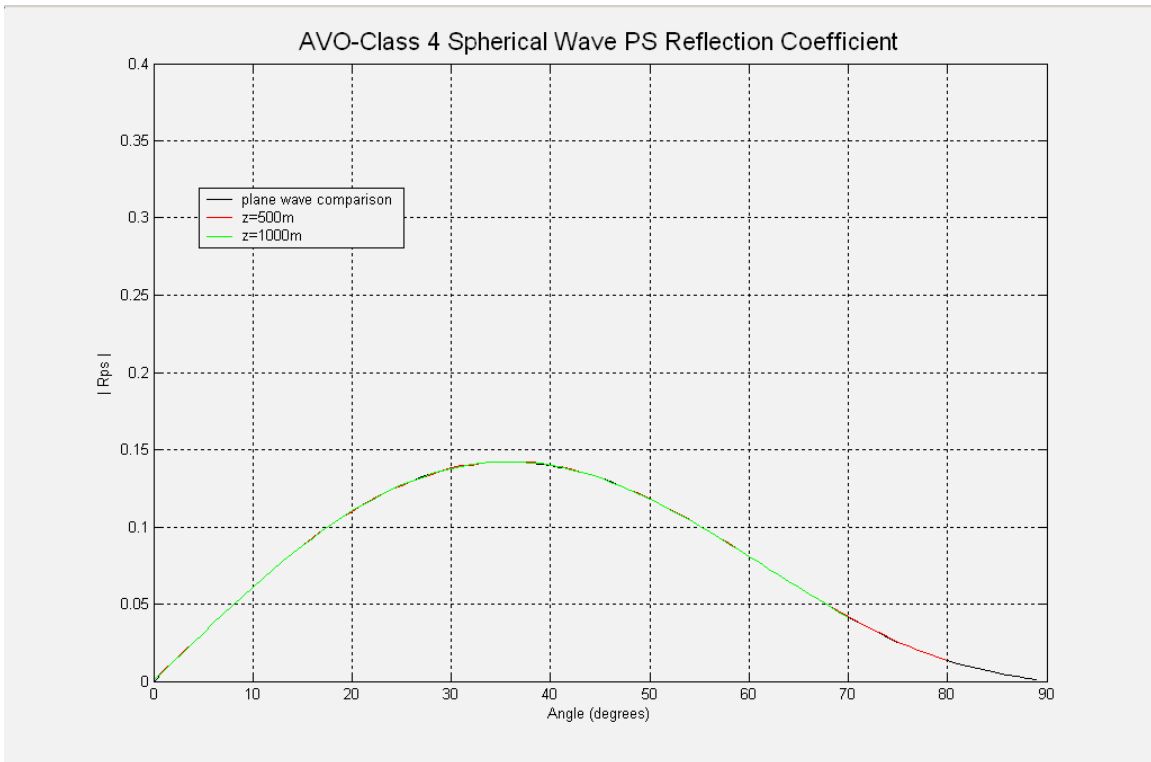


FIG. 4a. PS reflection coefficient curves for Class 4 AVO.

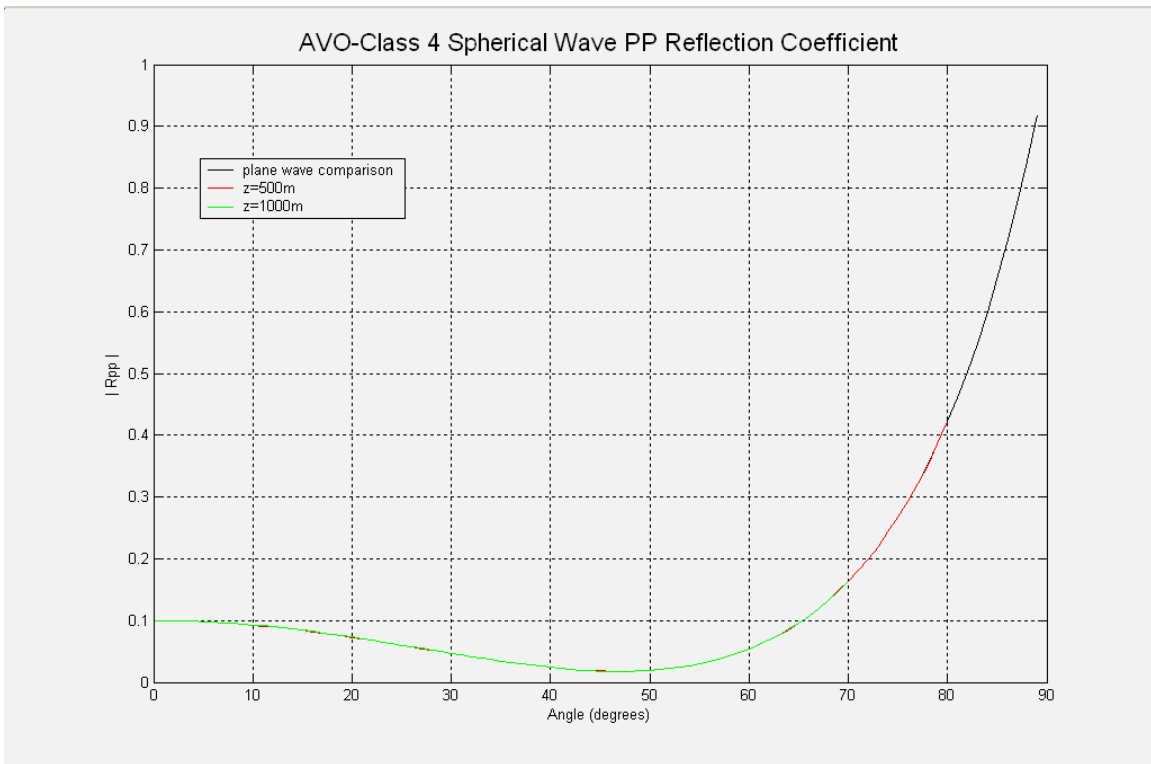


FIG. 4b. PP reflection coefficient curves for Class 4 AVO.

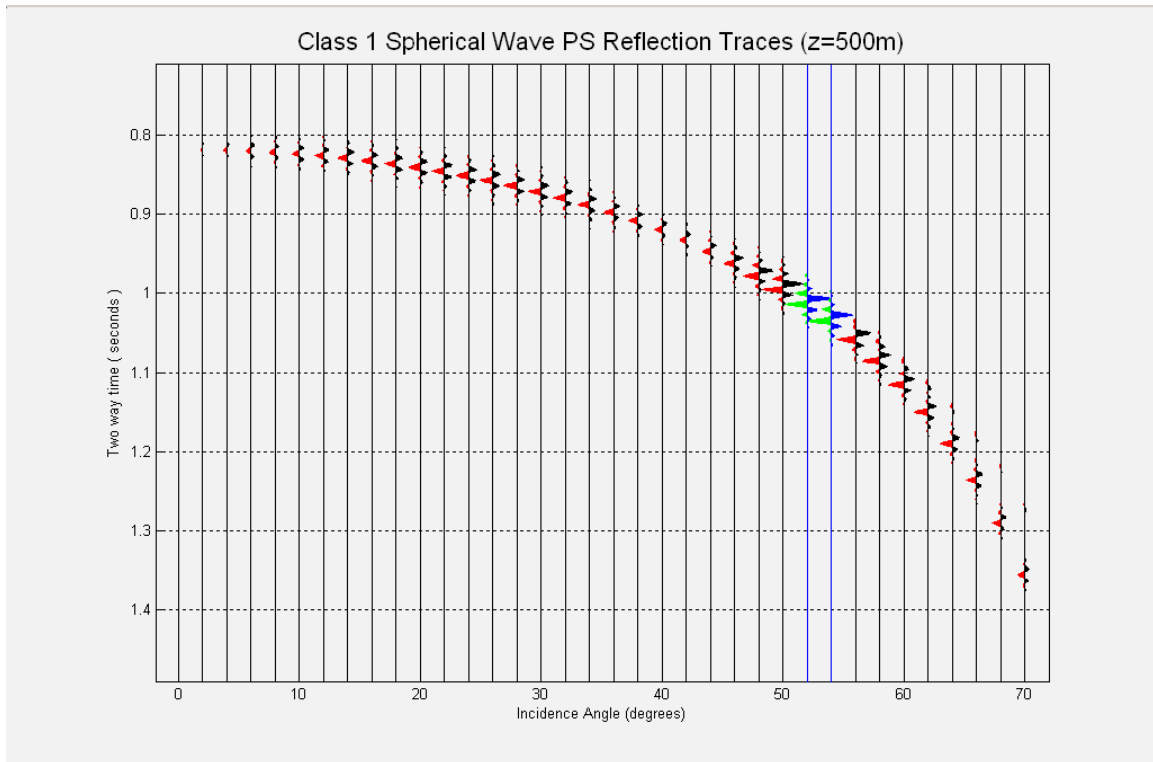


FIG. 5a. PS reflection traces for Class 1 AVO.

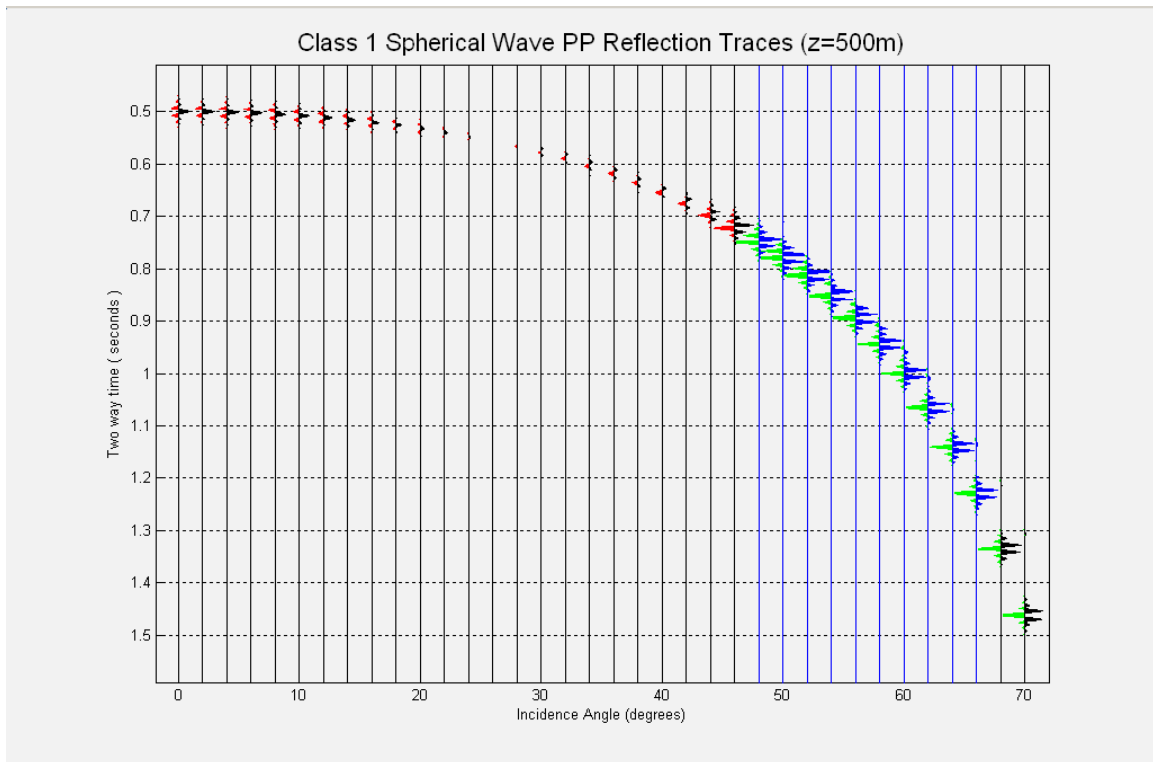


FIG. 5b. PP reflection traces for Class 1 AVO.

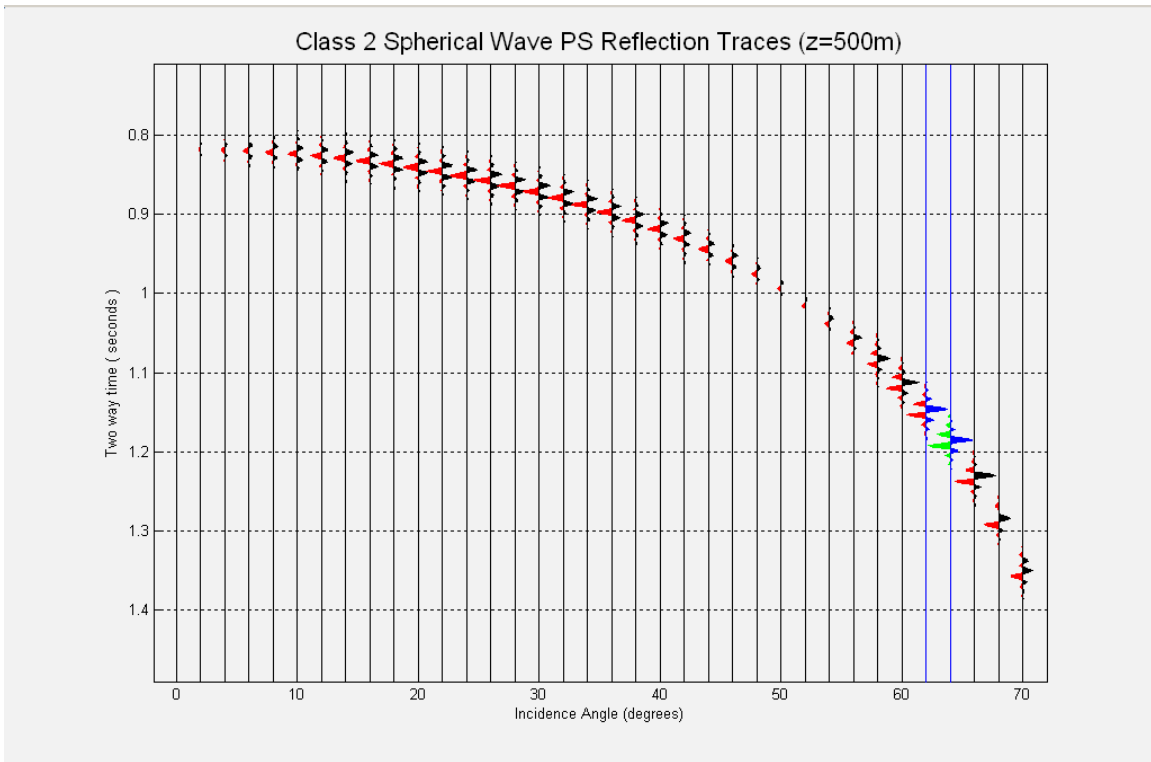


FIG. 6a. PS reflection traces for Class 2 AVO.

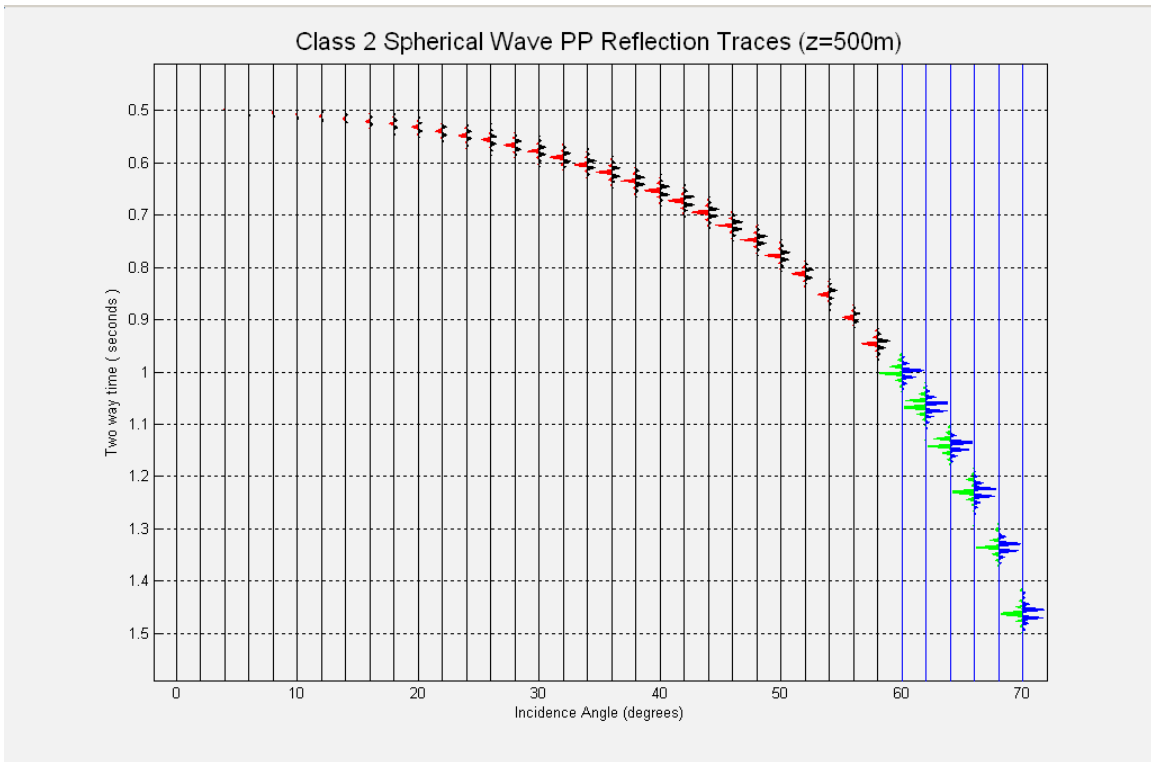


FIG. 6b. PP reflection traces for Class 2 AVO.

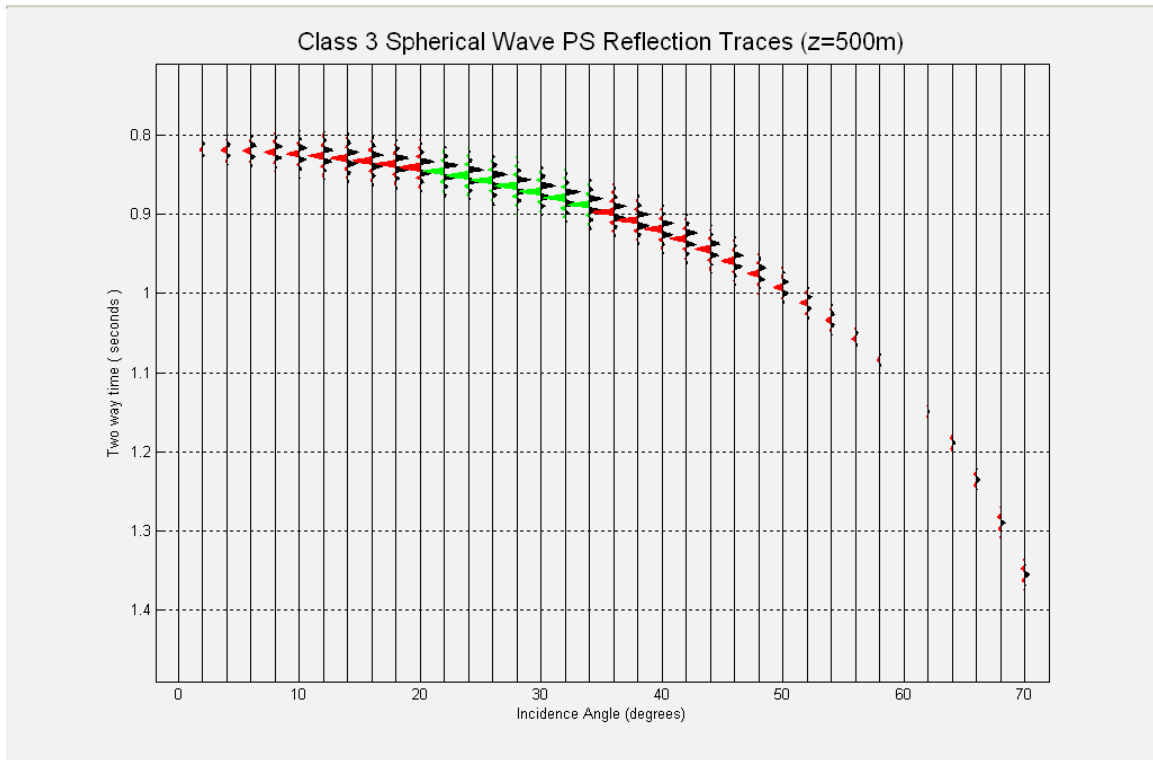


FIG. 7a. PS reflection traces for Class 3 AVO.

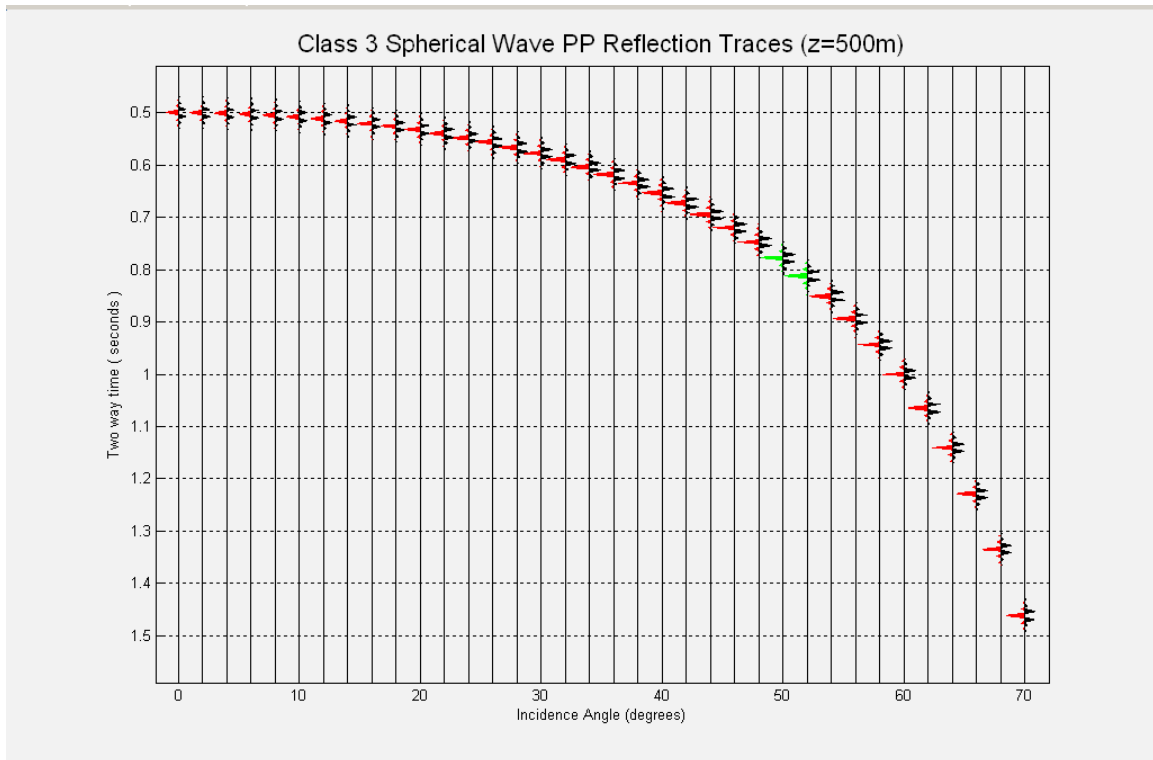


FIG. 7b. PP reflection traces for Class 3 AVO.

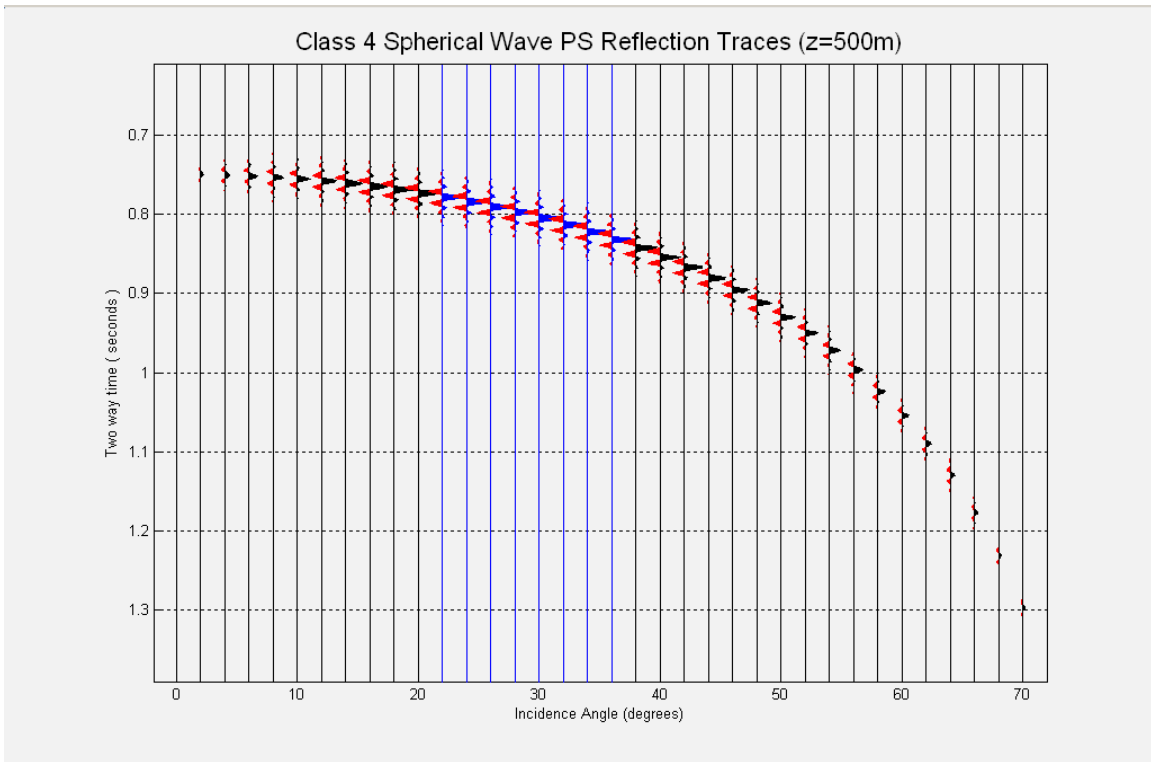


FIG. 8a. PS reflection traces for Class 4 AVO.

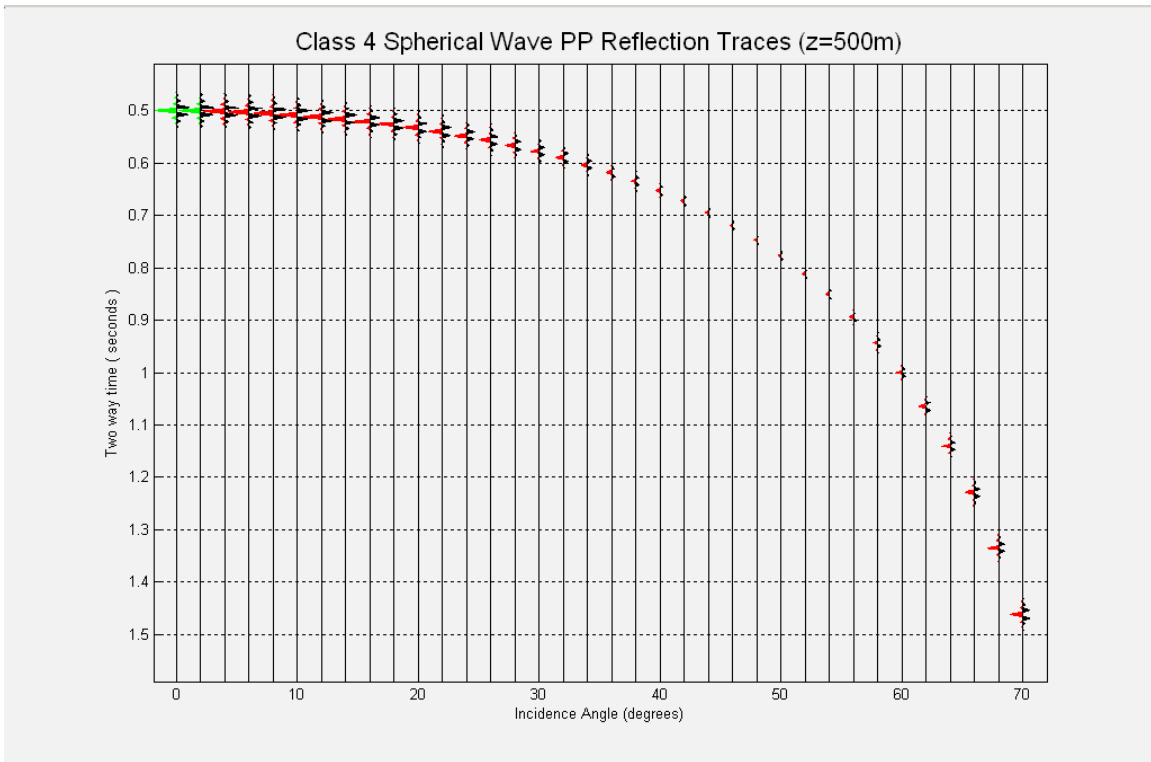


FIG. 8b. PP reflection traces for Class 4 AVO.

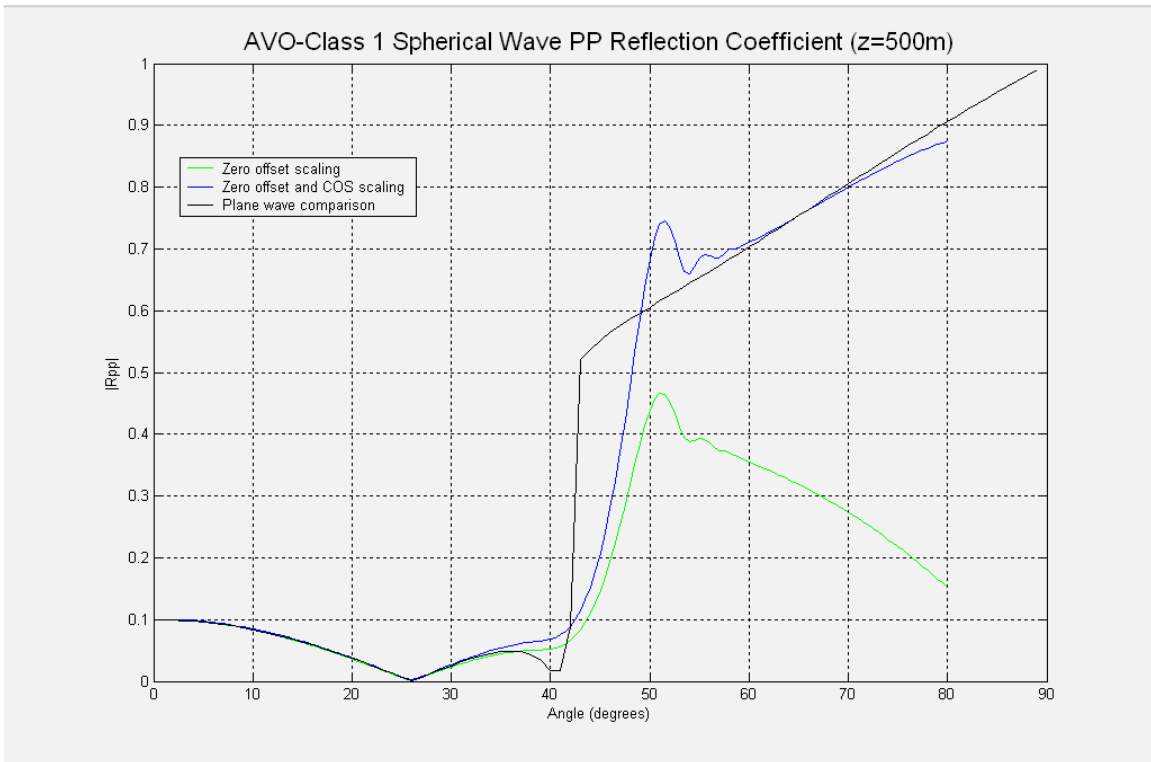


FIG. 9. Scaling comparisons for Class 1 PP-AVO.

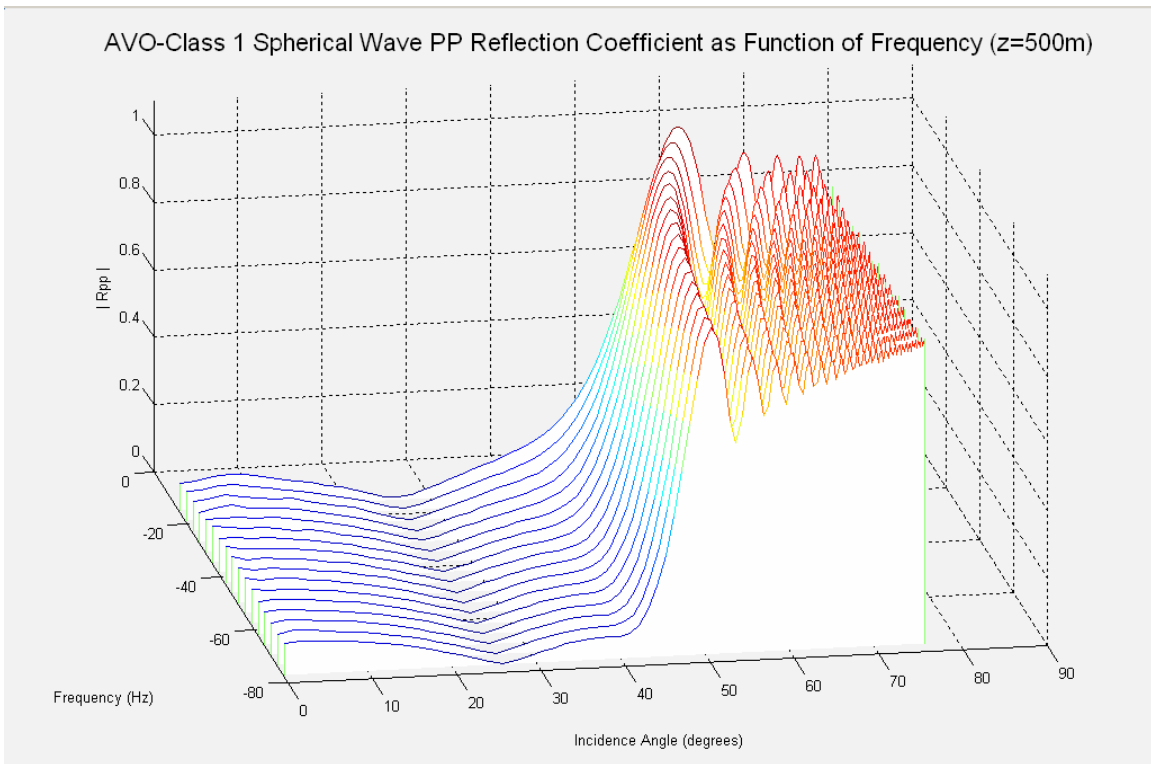


FIG. 10. Frequency dependence of Class 1 PP reflection coefficients.